Vol. 40, No. 3 (2018) 433-439, DOI: 10.24874/ti.2018.40.03.09

Tribology in Industry

www.tribology.rs

RESEARCH

Thermal Treatment Effect on Tribological and Corrosion Performances of 13Cr5Ni2Mo Super-Martensitic Stainless Steel

S. Tlili[a], N.E. Beliardouh[b], C.E. Ramoul[a,b], R. Bahi[b], O.I. Abdullah[c], H. Kaleli[d], M.A. Samad[e]

[a] *Research Center in Industrial Technologies CRTI P.O.Box 64, Cheraga 16014 Algiers, Algeria,*
[b]*Laboratoire Ingénierie des Surfaces (LIS), Université Badji Mokhtar, BP 12, 23000, Annaba, Algeria ,*
[c]*Department of Energy Engineering, College of Engineering, University of Baghdad, Iraq,*
[d]*Faculty of Mechanical Engineering, Automotive Division, Yıldız Technical University, Istanbul, Turkey,*
[e]*Department of Mechanical Engineering, King Fahd University of Petroleum and Minerals, Dhahran – 31261, KSA.*

Keywords:

Martensitic Stainless Steel
Thermal Treatments
Wear
Corrosion

Corresponding author:

Nasser Eddine Beliardouh
Laboratoire Ingénierie des Surfaces (LIS), Université BADJI Mokhtar, BP 12, 23000, Annaba, Algeria.
E-mail: beliardouh_23@yahoo.fr

A B S T R A C T

Wear behavior of 13Cr5Ni2Mo supermartensitic stainless steel (SMSS) were investigated in air and in argillaceous paste at room temperature. Prior to wear testing, the samples were subjected to two thermal treatments, namely; quenching followed by double tempering. A pin-on-disc test rig was used to conduct the wear test with a tribo-pair consisting of supermartensitic stainless steel sliding against itself. It was observed that the microstructure of the thermally treated samples mainly consisted of tempered martensite and carbides. Wear results showed that oxidative and abrasive wear dominated the wear process of the treated samples in both dry conditions and in argillaceous paste. Additionally corrosion tests were performed in 5.0% NaCl solution via potentiodynamic polarization tests. It was found that the passive film formation provides a good corrosion resistance to the samples.

1. INTRODUCTION

Recently, there has been an increasing demand for materials with high mechanical strength combined with high corrosion resistance to be used in different engineering fields, hydropower applications, water turbines and especially in the petroleum industry for flow lines (tube) in deep oil and gas wells, transporting fluid crude oil or gas at very high temperature and pressure. Low carbon super martensitic stainless steels (SMSS)containing more than 13% Cr, and alloyed with Ni, Mo, Nb, V, are considered to be a promising material for the above mentioned fields.

Alloying elements provide fine martensitic microstructure strengthened by carbide precipitations and avoid embrittlement during long term operation as reported by numerous works [1-3]. Nickel and Molybdenum are added for increasing resistance against pitting corrosion [4] while elements such as Ti, Nb and V are usually added to react with carbon individually, or react

with both carbon and nitrogen to form carbides and carbo-nitrides respectively resulting in an increase in strength [1]. Mechanical properties such as hardness and strength that are obtained by bulk heat treatment (quenching and tempering) depend on the amount of carbon introduced in the material [3,5,6]. Multiple alloying strategies and thermomechanical processing routes have been developed to achieve suitable blends of microstructure [7]. However, the formation of microstructure in SMSS steel with combination of mechanical properties required for industrial pipe processing mainly depends on the parameters of deformation and thermal treatments [8].

In oil exploration sites, SMMS tubes are assembled together by screwing (male/female coupling) while the drilling processes continue. Each, tube has the shape of a hollow cylinder with a screw thread. However, after a high number of usage cycles (assembling/dismantling) during their operation (SMMS against SMMS tribo pair) the screw thread is subjected to severe wear. Mostly, it can be attributed to the deterioration in tubes due to the synergistic effects that lead to the plastic deformation which is induced by the clamping and the corrosive action while using muddy waters.

The SMSS have moderate corrosion resistance in NaCl solution [9]. However the synergic effect of Cl- ions and H_2S lead to a rapid deterioration of the corrosion resistance [10].

Based on the available literature, there is absolutely no information about the tribological behavior of SMSS rubbing against itself. Hence, this research paper is focused on the microstructure characterization after thermal treatment, in order to improve the understanding of the tribological and corrosion behaviors of 13Cr5Ni2Mo Super-Martensitic Stainless Steel in the selected environment.

2. MATERIALS AND METHODS

2.1. Materials

The material used for this study was low carbon super martensitic stainless steels (SMSS). Specimens were cut from seamless hot-deformed tubes provided by *Oil Company of* Algeria-*SONATRACH*. The nominal chemical composition in weight percent of martensitic stainless steel samples, as provided by the manufacturer are listed in Table 1.

Table 1. The chemical composition of the tested samples.

Sample	Chemical composition [Wt. %]				
	C	**Mn**	**Si**	**P**	**S**
13Cr5Ni2Mo	0.018	0.411	0.215	0.011	0.004
	Cr	**Ni**	**Cu**	**Mo**	**Fe**
	12.25	5.45	0.245	2.06	bal

2.2. Wear tests

Both of the discs and the pins are machined from bars of 13Cr5Ni2Mo steel in the form of a cylinder (Fig. 1a). The thermal treatment process applied to the samples consisted of quenching from 1250 °C in an oil bath to room temperature followed by double tempering at 650 °C and air cooling. The first operation was conducted in two steps; specimens were heated slowly from room temperature to 850 °C and were held at the temperature for 30 min (temperature homogenization). After that they were further heated to 1250 °C and held at 1250 °C for 90 min to ensure a total austenisation of steel structure as presented in Fig. 1b. All of the thermal treatments are conducted in a horizontal tube furnace under a flow of argon protective atmosphere.

Tribological tests were conducted on a tribometer (*CSM HT1000*) using a pin-on-disc configuration in which the specimen acts as the disc that rotates in contact with a static partner (Fig. 1c). Tests were conducted under dry conditions and also while immersing the specimen in argillaceous paste. The clay paste is composed of 50 g of bentonite in 100 ml H_2O (distilled water). Table 2 presents the tribological test parameters. The surface morphology of the tested specimens was analyzed by optical and scanning electron microscopy (SEM/EDS; *JEOL JSM 6830*).

The volumetric wear rate (K) was calculated using an optical profilometer (*Veeco-Wyko NT1100*) according to the conventional formula (1):

$$K = \frac{V}{L.N} \quad (1)$$

Where K is the specific wear rate [mm^3/Nm], V is the volume loss [mm^3], N is the normal load [N] and L is the sliding distance [m].

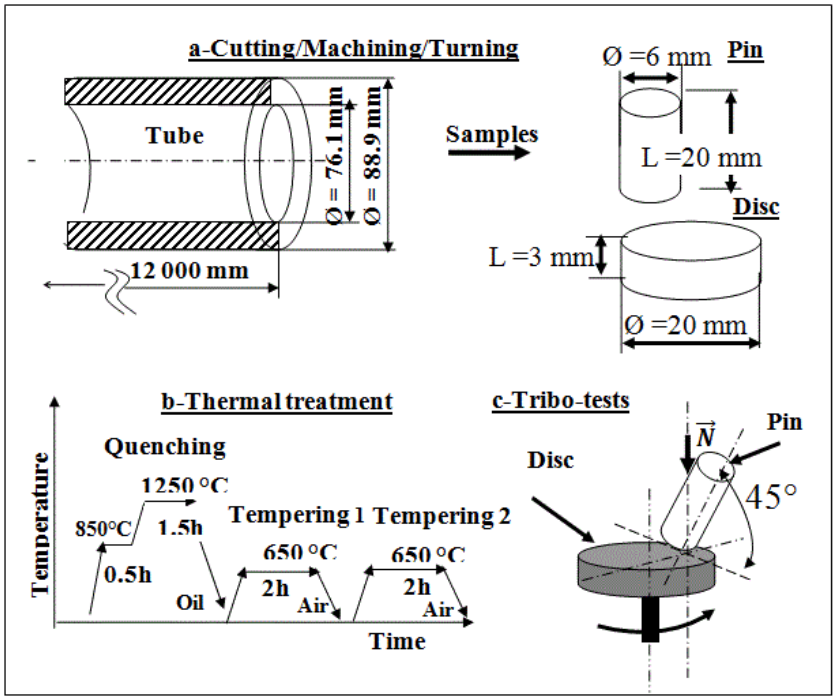

Fig. 1. a - Specimen preparation from pipe before thermal treatments and tribo-tests, b - Exemplified processing steps in a time–temperature overview, c - Pin-on-disc wear test configuration.

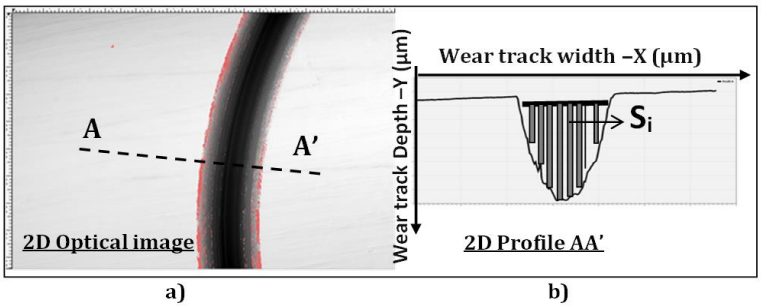

Fig. 2. Quantitative analysis of wear: a) Optical image of wear track (*Gwyddion* software image) and (b) Example of extracted profile across the line AA'.

Table 2. Pin-on-disc test parameters.

Parameters	Select value
Velocity (cm/s)	2
Applied load (N)	5
Total sliding distance (m)	20
Wear track diameter (mm)	4
Environment	Air
Temperature (°C)	20 ± 3
Humidity (%)	40 ± 5

The wear volume (volume loss) was estimated by measuring the surface profiles across the wear track at different locations. At each location, for example location -AA'- as shown in figure 2(a-b), a XY profile (2D profile: width/depth in µm) was extracted and the surface area S_i was calculated by the following equation (2):

$$S_i = \sum_{i=0}^{n}[(x_{i+1} - x_i).(y_i)] \quad (2)$$

The volume loss was automatically calculated as the surface area S (Equation (3)) multiplied by the circumference, 2πr where r is the track radius -Table 2.

$$S = \sum S_i \quad (3)$$

2.3 Electrochemical tests

Electrochemical tests were conducted in two aqueous saline solutions; a 5.0 (wt. %) NaCl in distilled water and 5.0 (wt. %) NaCl + 0.5M N_2SO_4 in distilled water. Conventional three-electrode cells consisting of saturated calomel reference electrode (SCE), platinum counter electrode and the tested specimen as the working electrode (1.0 cm^2 of exposed area) was used. All experiments

were conducted under free air (natural convection) at room temperature (25 °C) using a *GAMRY Model PCI 4* unit.

Tafel polarization curves were obtained at a sweep speed of 0.5 mV/s, and the voltage was in the range of –1.0 to +1.0 V/ECS. Before starting the tests, all the samples were stabilized in the 5.0 (wt.%) NaCl solution for 2h, in order to attain a stable open circuit electrode potential (OCP). The selected 5.0 (wt.%) NaCl solution is a standard test medium. It is well known as a strong aggressive solution that causes deep corrosion damage to many metallic alloys including stainless steels. The addition of Na_2SO_4 is based on its inhibition effect on pitting corrosion of stainless steels as reported in literature [9,11].

3. RESULTS AND DISCUSSION

3.1 Microstructure

Metallographic analysis was conducted using an optical microscope (*Nikon Eclipse LV100ND).* Figure 3 shows the optical microstructure obtained after thermal treatments. It consists of tempered martensite laths and fine carbide precipitates. A few quantities of retained austenite were also found along the grain boundaries. SEM/EDS analysis showed that carbides were mainly constituted of (Mo, Cr, $Fe)_{23}C_6$. Precipitation of carbides may occur both at grain boundaries and within the grains. This microstructure was encountered and described by many researchers [1,8,12].

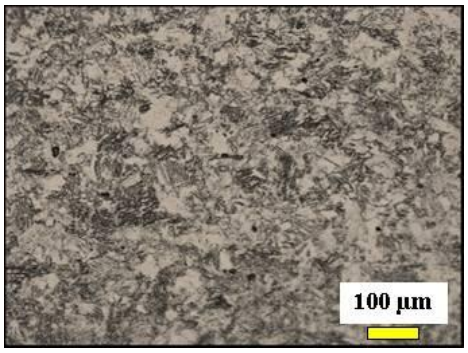

Fig. 3. Optical microstructure of the tested specimen.

The hardness value measured after the heat treatment was found to be 26 ±2 HRC, while the range of yield strength and tensile strength were found to be (850 ±2MPa) and (950 ±2MPa) respectively. The elongation reached to 20 %, in the tensile tests which were conducted according to the ASTM E8 standards. Three tests were done for repeatability.

3.2 Tribological behaviour

Figure 4 presents the variation of the coefficient of friction (COF) when testing samples under the dry and argillaceous paste conditions respectively. The COF started with a low value, approximately 0.2 in all cases, and then reached a steady-state value of 1.1 (under dry conditions) and 0.5 (in argillaceous paste) after 5 m of sliding distance.

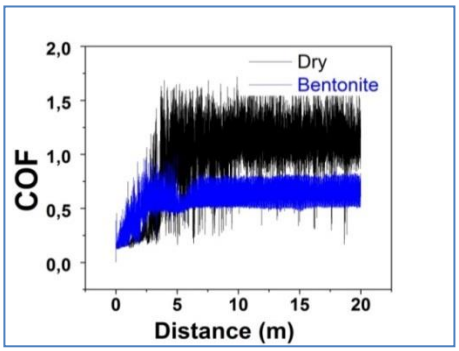

Fig. 4. Coefficient of friction evolutions.

During the steady-state period, the COF remained constant. This can be attributed to an oxide film formed on the contact surfaces (SMSS vs. SMSS), that transforms into debris because it becomes brittle after some cycles of sliding. Thus, the contact surfaces were abraded by the wear debris (second state) when they rubbed together.

In argillaceous paste medium, the metal couple in contact produced low COF, lower than that observed in dry conditions. The obtained average values of wear rates are K_1= (8.38±1.2) $.10^{-7}$mm^3/Nm and K_2= (1.26±0.5) $.10^{-8}$ mm^3/Nm in dry and argillaceous paste medium, respectively.

This is clear evidence that the test conditions in the present study were in the friction domain. The argillaceous paste based bentonite used in this study, did not play any role as a lubricant.

3.3 Wear mechanisms

Tests in dry conditions

Figure 5 illustrates the typical wear track morphologies. It can be seen that the wear

tracks is characterized by wear debris (white particles) and deep grooves (and ridges) parallel to the sliding direction. Severe plastic deformation was observed on the surfaces of the specimen when tested under the dry condition. The plastic deformation pathlines are clearly visible in Fig. 5b, suggesting that the surface material was subjected to high contact pressure. Moreover, EDS analysis also revealed the presence of SMSS specimen elements and oxygen i.e. Fe, Cr, Ni, C, Mo and O, indicated by label "1". These debris are the result of the fragmentation of the surface oxide layer which formed as a consequence of an increase in temperature during sliding. No cracks were observed on the formed grooves which proved the high resistance of shearing and strengthening of the surface sublayers of SMSS. Removal of hard particles (carbides) from the matrix, leave voids and holes as shown in Fig. 5b (indicated by yellow arrows). Such features are characteristics of abrasion wear [13], in which hard asperities and/or hard particles plough through the SMSS specimens, suggesting that, the main wear mechanism is a third body abrasive wear.

Tests in argillaceous paste conditions

Figure 6a exhibits the worn surface of samples tested in the argillaceous paste medium. Grooves parallel to the sliding direction and wear debris can be observed. EDS analyses showed that wear debris are composed of carbides and oxides, suggesting that, the abrasion is the main wear mechanism. During abrasion, material removal from the surface occurs by ploughing. Figure 6b shows the formation of ridges. Furthermore, flaws caused by individual particles, probably primary carbides removed from the matrix, are clearly seen (indicated by yellow arrows). Hence, oxidative and abrasive (third body) wear are found to be the main mechanisms involved when two surfaces of SMSS are sliding together under argillaceous paste conditions.

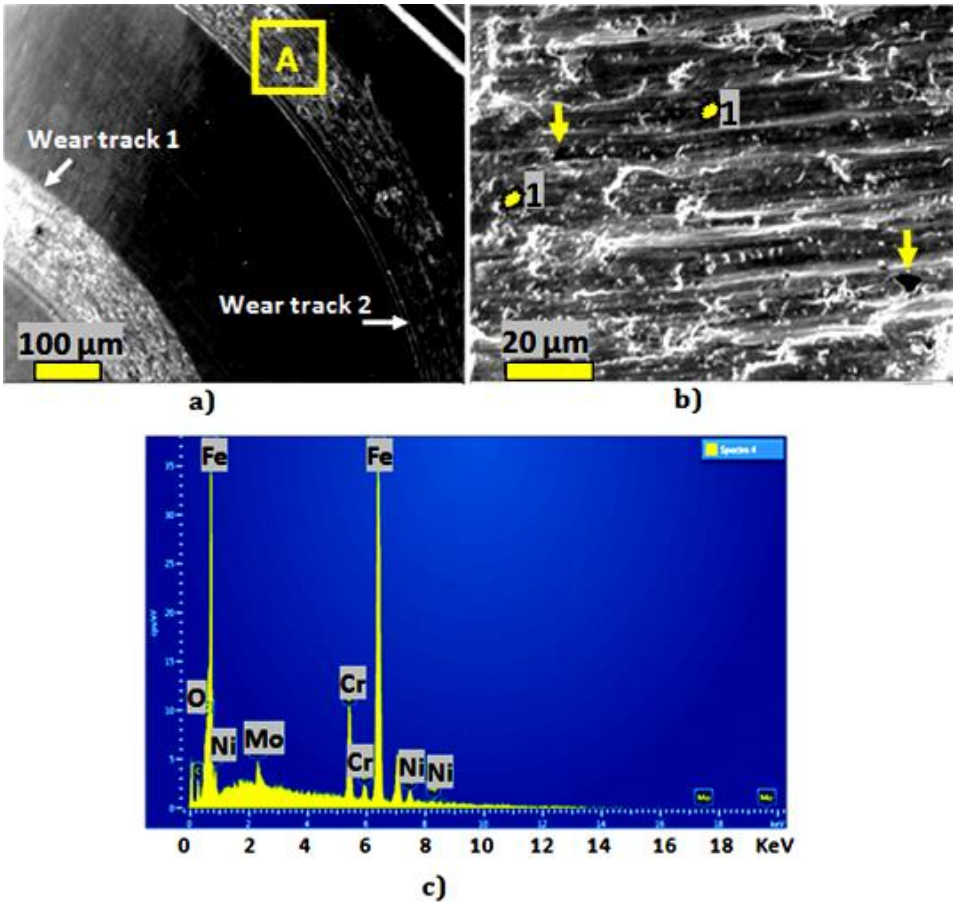

Fig. 5. SEM micrographs: a) General overview of the wear tracks morphologies of SMSS samples tested in unlubricated conditions, b) Zoom of the area in square A, and c) EDS spectrum obtained at point "1".

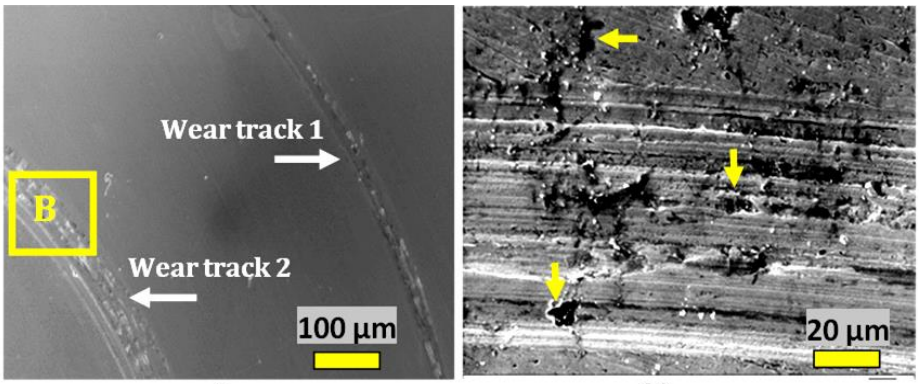

Fig. 6. SEM micrographs: a) General overview of the wear tracks morphologies of SMSS samples tested in argillaceous paste conditions, and b) Zoom of the area in square B.

Table 3. Summary of potentiodynamic polarization test results.

13Cr5Ni2Mo	I_{corr} (µA/Cm²)	E_{corr} (mV)	b_a (mv)	b_c (mv)	R_p (Ohm)
5% NaCl	0.989	-329.75	385.3	117.8	37172
5% NaCl + 0,5 M Na_2So_4	2.03	-339.91	334.8	119.2	23715

Finally, it can be concluded that the same mechanisms of wear are observed under both dry and argillaceous paste conditions. The difference in the wear rates can be attributed to the microstructure and its features. On one hand, high chemical reactivity of the surface, resulting in rapid surface oxidation occurs in the first state of wear as a consequence of high interface temperature [14], which leads to an oxidative wear. On the other hand, martensitic microstructure modifications (hardening) of the surfaces in contact leads to a rapid and easy fragmentation of the top layers. These two phenomena occur differently in dry and wet conditions, thus acting on the friction between the mating pairs subjected to wear. In the second state, the main mechanism involved was found to be abrasive wear.

3.4 Corrosion performances

Figure 7 displays the potentiodynamic polarization curves of the SMSS samples in both NaCl and NaCl + Na_2SO_4 aqueous solutions. The corrosion current density (I_{corr}) and the corrosion potential (E_{corr}), were determined using the Tafel extrapolation method while the Sterne-Geary equation [15] was used to calculate the polarization resistance (R_p). The results can be seen in Table 3.

For both the tested mediums, all samples showed a large plateau in the anodic region-0.35 up to 0.17 V/ECS and from -0.35 up to +0.27 V/ECS corresponding to a passive oxide film formation. After that, failure in the film occurred (point 1 and point 1') characterized by an increase in the slope of the anodic curve. In the cathodic domain, a pseudo plateau was also observed due to oxygen reduction.

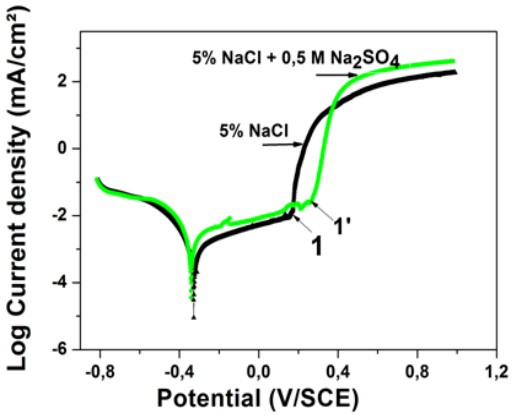

Fig. 7. Linear polarization curves plotted after 2h of immersion in aggressive mediums.

Finally, it was found that all specimens showed a better corrosion resistance against chloride ions $(Cl)^-$, with lower (I_{corr}) and higher R_p values. The influence of sulfate ions $(SO4)^{2-}$ is clearly seen by the largest anodic passivity plateau in the case of NaCl + Na_2SO_4 solution i.e. the polarization curves shifted to the more positive direction.

4. CONCLUSIONS

The results obtained from the present work can be summarized as follows:

1. Based on the specific wear rates it was found that the dry sliding produced severe wear. However, the friction reduced when the tests were carried out in the argillaceous paste medium, without causing any changes to the wear mechanisms. In all cases, a third body abrasive wear is observed in the SMSS *vs*. SMSS contact pair.
2. Strong passive behaviour was observed on SMSS in 5.0 % NaCl and 5.0 % NaCl+ 0.5M Na_2SO_4 solutions whereby corrosion species were not able to penetrate the oxide film.
3. The suggested thermal treatments of quenching followed by double tempering significantly improved the wear resistance of SMSS. It also helped in improving the corrosion resistance of SMSS in aggressive medium containing chloride ions.

REFERENCES

[1] X. Ma, B. Langelier, B. Gault, S. Subramanian, *Effect of Nb Addition to Ti-Bearing Super Martensitic Stainless Steel on Control of Austenite Grain Size and Strengthening*, Metallurgical and Materials Transactions A, vol. 48, iss. 5, pp. 2460-2471, 2017, doi: 10.1007/s.11661.017.4036.7

[2] Y. Sun, *Sliding Wear Behaviour of Surface Mechanical Attrition Treated AISI 304 Stainless Steel*, Tribology International, vol. 57, pp. 67–75, 2013, doi: 10.1016/j.triboint.2012.07.015

[3] Y.-r. Liu, D. Ye, Q.-l. Yong, J. Su, K.-y. Zhao, W. Jiang, *Effect of Heat Treatment on Microstructure and Property of Cr13 Super Martensitic Stainless Steel*, Journal of Iron and Steel Research International, vol. 18, iss. 11, pp. 60-66, 2011, doi: 10.1016/s.1006.706x(11).60118.0

[4] A. Pfenning, A. Kranzmann, *Potential of Martensitic Stainless Steel X5CrNiCuNb 16-4 as Pipe Steel in Corrosive CCS Environment,* International Journal of Environmental Science and Development, vol. 8, no. 7, pp. 466-473, 2017, doi: 10.18178/ijesd.2017.8.7.998

[5] D. Zou, X.H. Liu, Y. Han, W. Zhang, J. Li, K. Wu, *Influence of Heat Treatment Temperature on Microstructure and Property of Cr13Ni5Mo2 Supermartensitic Stainless Steel*, Journal of Iron and Steel Research, International, vol. 21, no. 3, pp. 364-368, 2014, doi: 10.1016/S1006-706X(14)60056-X

[6] D.-k. Xu, Y.-c. Liu, Z.-q. Ma, H.-j. Li, Z.-s. Yan, *Structural Refinement of 00Cr13Ni5Mo2 Supermartensitic Stainless Seel During Single-Stage Intercritical Tempering*, International Journal of Minerals, Metallurgy and Materials, vol. 21, iss. 3, pp. 279-288, 2014, doi: 10.1007/s12613-014-0906-9

[8] M. Belde, H. Springer, G. Inden, D. Raabe, *Multiphase Microstructures Via Confined Precipitation and Dissolution of Vessel Phases: Example of Austenite in Martensitic Steel*, Acta Materialia, vol. 86, pp. 1–14, 2015, doi: 10.1016/j.actamat.2014.11.025

[9] I.Y. Pyshmintsev, S.M. Bityukov, V.I. Pastukhov, M.L. Lobanov, *Evolution of Microstructure Stainless Martensitic Steel for Seamless Tubing*, in International Conference on Mechanics, Resource and Diagnostics of Materials and Structures, (MRDMS-2017), 11–15, December 2017, Ekaterinburg, Russia, AIP Conference Proceedings, vol. 1915, no. 1 , 040048, 2017, doi: 10.1063/1.5017396

[10] S. Marcelin, N. Pébèrea, S. Régnier, *Electrochemical Characterisation of a Martensitic Stainless Steel in a Neutral Chloride Solution*, Electrochimica Acta, vol. 87, pp. 32– 40, 2013, doi: 10.1016/j.electacta.2012.09.011

[11] S. Zhu, J. Li, C. Wang, L. Yang, *Corrosion Behaviour of 00Cr13Ni5Mo2 Domestic Super Martensitic Steel in the Presence of Elemental Sulphur*, Revista Técnica de la Facultad de Ingeniería Universidad del Zulia, vol. 38, no. 1 , pp. 10-16, 2015.

[12] M.D. Pereda, C.A. Gervasi, C.L. Llorente, P.D. Bilmes, *Micro Electrochemical Corrosion Study of Super Martensitic Welds in Chloride-Containing Media*, Corrosion Science, vol. 53, iss. 12, pp. 3934–3941, 2011, doi: 10.1016/j.corsci.2011.07.040

[13] A. Dalmau, W. Rmili, D. Joly, C. Richard, A. Igual-Munoz, *Tribological Behavior of New Martensitic Stainless Steels Using Scratch and Dry Wear Test*, Tribology Letters, vol. 56, iss. 3, pp. 517–5295, 2014, doi: 10.1007/s11249-014-0429-6

[14] Z. Doni, M. Buciumeanu, L. Palaghian, *Topographic and Electrochemical Ti6Al4V Alloy Surface Characterization in Dry and Wet Reciprocating Sliding*, Tribology in Industry, vol. 35, no. 3, pp. 217-224, 2013.

[15] A. Elhadi, A. Bouchoucha, W. Jomaa, Y. Zedan, T. Schmitt, P. Bocher, *Study of Surface Wear and Damage Induced by Dry Sliding of Tempered AISI 4140 Steel Against Hardened AISI 1055 Steel*, Tribology in Industry, vol. 38, no. 4, pp. 475-485, 2016.

[16] F. Mansfeld, *The Polarization Resistance Technique for Measuring Corrosion Currents*, in M.G. Fontana, R.W. Staehle (Ed.): Advances in Corrosion Science and Technology, Springer, Boston, MA , pp. 163-262, 1976.